https://doi.org/10.22226/2410-3535-2022-4-282-286

Effect of carbon alloying on hydrogen embrittlement of a Cantor alloy

M. Yu. Panchenko[†,1], E. V. Melnikov[1], D. Yu. Gurtova[1,2], E. G. Astafurova[1]

[†]panchenko.marina4@gmail.com

[1]Institute of Strength Physics and Materials Science, SB of RAS, Tomsk, 634055, Russia
[2]National Research Tomsk State University, Tomsk, 634050, Russia

We have investigated the effect of hydrogen-charging on the mechanical properties and fracture mechanisms of high-entropy alloys $Fe_{20}Mn_{20}Cr_{20}Ni_{20}Co_{20}$ and $Fe_{20}Mn_{20}Cr_{20}Ni_{20}Co_{19}C_1$ (at.%). Both alloys have a coarse-grained single-phase face-centered cubic (fcc) structure. It was found that doping with carbon decreases the content of hydrogen absorbed by the specimens during electrochemical hydrogen-charging (in a 3% NaCl water solution, at j=10 mA/cm^2 for 50 h): 134 wppm and 63 wppm for carbon-free and carbon-doped alloy, respectively. Hydrogen-charging contributes to an increase in the yield strength and a decrease in the ductility of the alloys. Despite the lower concentration of dissolved hydrogen, the hydrogen-associated solid-solution strengthening of the carbon-doped alloy is higher than that in the interstitial-free alloy. The hydrogen embrittlement index, I_H=17%, for carbon-alloyed specimens is lower than I_H = 25% for interstitial-free specimens. In both alloys, the hydrogen-affected surface layers of the specimens fracture in a similar brittle mode — intergranular fracture dominates.

Keywords: hydrogen embrittlement, high-entropy alloys, interstitial hardening, carbon, fracture.

1. Introduction

It is generally recognized that hydrogen degrades the mechanical properties of metals, leading to a decrease in ductility and bearing capacity, significantly reducing the operating life of the material. The issue of hydrogen embrittlement is reflected in industries related to the energy storage and conversion, such as hydrogen energy, oil and gas transportation, operation of wind turbines for electricity generation and nuclear power [1]. Therefore, the search for materials that are resistant to the deleterious effects of hydrogen is of great importance.

A new class of materials, high-entropy alloys (HEA), is currently attracting the attention of many researchers. Due to their unique physical and mechanical properties, they have a potential application in extreme service environments [2]. One of the wide-spread and frequently investigated high-entropy alloy is the five-component equimolar CoCrFeMnNi Cantor alloy [3,4]. It is a single phase face-centered cubic (fcc) solid-solution with high thermodynamic stability, very high tensile elongation and exceptional fracture toughness at low temperatures [4,5].

Y. Zhao et al. shown [6] that the resistance of the CoCrFeMnNi alloy to hydrogen embrittlement is higher than that of stable austenitic stainless steel under gaseous hydrogen charging. Luo et al. [7] reported that hydrogen charging can even slightly improve the strength and ductility of the alloy. At the same time, there are number of works [8–10] reporting the susceptibility of the HEAs to hydrogen embrittlement. Yet, the phenomenon of the hydrogen embrittlement in HEAs, in particular, in the Cantor alloy, has not been fully explored.

Besides, the limitation of the fcc HEAs as an engineering material due to the low yield strength [4,5] stimulates the research of interstitially-alloyed HEAs, in particular, the carbon-alloyed Cantor alloy. Due to the solid-solution strengthening and precipitation hardening, the addition of carbon increases the strength of fcc HEAs without a significant loss of ductility [11–13]. Up to date, there are insufficient data on the effect of interstitial atoms on the hydrogen embrittlement of HEAs, and they are controversial. Luo et al. [14] claimed that C-doping increases susceptibility of the CoCrFeMnNi alloy to hydrogen embrittlement. The authors also noted that carbides, peculiar for major carbon-alloyed HEAs, act as potential sites for crack initiation in the carbon-alloyed HEA. Incomplete recrystallization with the presence of non-recrystallized zones and nanotwins in structure of $Co_{19.9}Cr_{19.9}Fe_{19.9}Mn_{19.9}Ni_{19.9}C_{0.5}$ (at.%) alloy increases the resistance to the harmful effects of hydrogen according to the research by H. Luo [15]. Fu et. al reported that carbon alloying (0.5 at.%) of a metastable FeMnCoCr high-entropy alloy contributes to a slight increase in resistance of the alloy against hydrogen embrittlement [16].

To clarify the interstitial-alloying effect on the hydrogen embrittlement in HEAs and to avoid precipitation-assisted impact, we have obtained two alloys possessing the single-phase structures — interstitial-free and carbon-alloyed Cantor alloys. Hence, the aim of this work is to reveal the effect of carbon alloying on the hydrogen embrittlement of a high-entropy CoCrFeMnNi alloy.

2. Materials and experimental methods

The materials used in this study were the equiatomic $Fe_{20}Mn_{20}Cr_{20}Ni_{20}Co_{20}$ (at.%, HEA) Cantor alloy and the interstitial carbon-alloyed $Fe_{20}Mn_{20}Cr_{20}Ni_{20}Co_{19}C_1$ (at.%, HEA-C) alloy. The cast HEA was subjected to a thermomechanical treatment (TMT): an annealing at a temperature of 1200°C for 2 hours, cold rolling (80% reduction) and final annealing at temperature of 1200°C for 2 hours followed by water-quenching. The TMT for HEA-C alloy included annealing at a temperature of 1200°C for 12 hours, hot forging at a temperature of 1230°C, second annealing at a temperature of 1200°C for 12 hours, cold rolling to obtain a thickness reduction to 80% and final annealing at a temperature of 1200°C for 1 hour following by water-quenching.

The dumbbell-shaped tensile specimens of $12.0\times2.6\times\times1.4$ mm^3 in gauge section were cut from the TMT-processed materials. After mechanical grinding, the specimens were electrolytically polished in supersaturated solution of chromium anhydride CrO_3 in phosphoric acid H_3PO_4. The specimens were tensile tested at room temperature and a strain rate of 5×10^{-4} s^{-1} using electromechanical machine LFM-125 (Walter+Bai AG, Switzerland).

The X-ray diffraction (XRD) analysis was done using DRON 7 diffractometer with Co-K_α radiation. Lattice parameters were obtained by extrapolating the dependence of a_{hkl}, determined for each X-ray line with indices (*hkl*), on the function ($\cos\theta\cot\theta$).

Electrochemical hydrogen-charging was conducted with a current density of 10 mA/cm^2 for 50 h in a 3% NaCl water solution containing 3 g/l of NH_4SCN as a recombination poison. Thermal desorption spectroscopy (TDS) was carried out in the temperature interval of 25 – 800°C with the heating rate of 6°C/min using a vacuum chamber with a simultaneous thermal desorption spectra collection by an RGA100 quadrupole mass spectrometer (Stanford Research Systems, USA). The hydrogen concentrations absorbed by the alloys were measured using a LECO ONH 836 analyzer.

The microstructure and fracture surfaces were characterized using a QUANTA 200 3D scanning electron microscope (SEM) equipped with an energy-dispersive analysis system and electron backscattered diffraction (EBSD) supply.

3. Results and Discussion

XRD patterns and EBSD grain maps of HEA and HEA-C specimens are presented in Fig. 1. Regardless of the alloy composition, the XRD-patterns contain diffraction peaks with interplanar distances corresponded to the austenitic phase. Carbon alloying leads to a shift of the diffraction peaks towards smaller angles. The analysis of the EBSD images and the XRD data indicates that both alloys have a single-phase coarse-grain fcc structure. Only single carbides ($M_{23}C_6$, M_7C_3) could appear in HEA-C specimens after TMT [17], and the low fraction of such carbides allows us to neglect their impact. The lattice parameter of the interstitial-free alloy is $a=3.598\pm0.006$ Å, and it is much higher in HEA-C, $a=3.611\pm0.002$ Å. An increase in the *a*-value indicates a solid-solution strengthening of the austenitic phase by carbon atoms (1 at.%). The average grain size of the Cantor alloy, $d=215\pm77$ μm, is larger than $d=128\pm59$ μm of the carbon-doped alloy.

Fig. 2 shows the bar plots comparing the mechanical properties (yield strength $\sigma_{0.2}$, ultimate tensile stress (σ_{UTS}) and elongation-to-failure) of hydrogen-free and hydrogen-charged specimens. Doping with carbon leads to a significant increase in the strength properties of the initial specimens (without hydrogen-charging). This is caused by solid-solution strengthening and grain refinement, as it was previously reported for multicomponent alloys with interstitial atoms in [3,11,13]. Carbon-alloying in accompanied with the decrease in elongation-to-failure of Cantor alloy. As we previously reported in [17], stress-strain diagrams for HEA-C specimens are more parabolic than those for the interstitial-free Cantor alloy, and strain hardening of the interstitial alloy is higher due to carbon-assisted increase in lattice friction stresses.

Hydrogen-charging contributes to the change in the mechanical properties of both alloys. The yield strength of the alloys increases after hydrogen-charging (Fig. 2). Such solid-solution strengthening by hydrogen was previously observed in other interstitial high-entropy alloys [10,14]. More pronounced change in the yield strength caused by hydrogen ($\Delta\sigma_{0.2}^{H}=22$ MPa for HEA-C, $\Delta\sigma_{0.2}^{H}=10$ MPa for HEA) is observed in carbon-dopped alloy (Fig. 2), which indicates higher solubility of hydrogen in the austenitic phase the of HEA-C specimens despite the smaller grain size and higher fraction of the grain boundaries. After

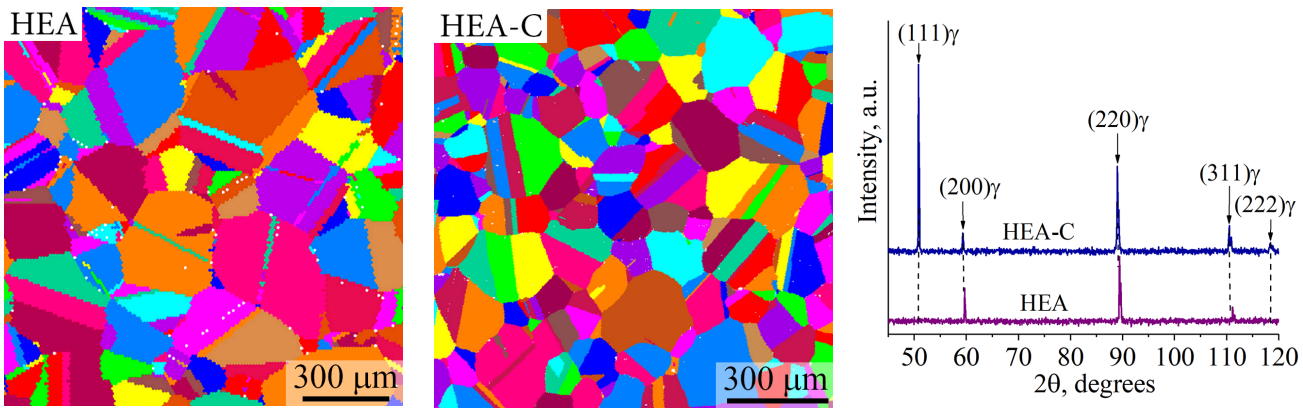

a b c

Fig. 1. (Color online) XRD patterns (a) and EBSD grain maps (b, c) of HEA (b) and HEA-C (c) specimens.

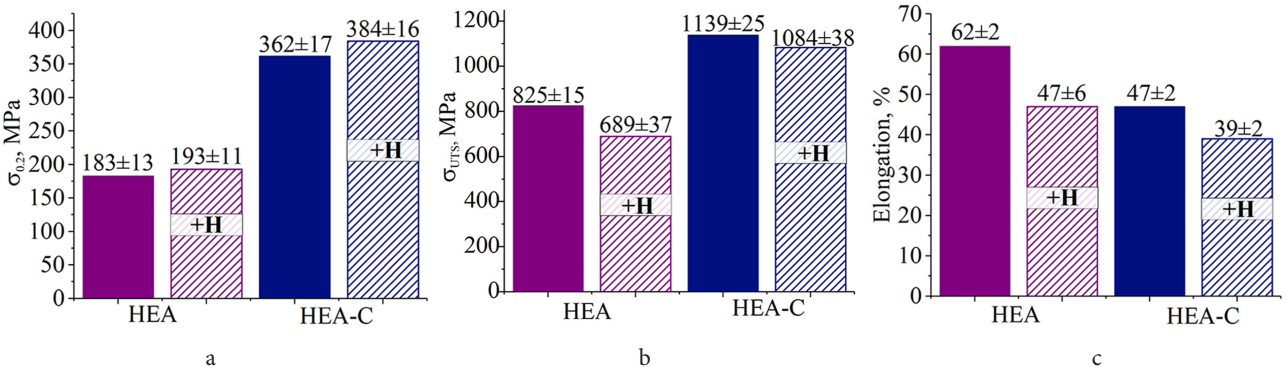

Fig. 2. (Color online) Bar plots of the yield strength ($\sigma_{0.2}$) (a), ultimate tensile stress (σ_{UTS}) (b) and elongation-to-failure (c) of hydrogen-free and hydrogen-charged HEA and HEA-C specimens. Data for hydrogen-charged specimens marked by "+H".

hydrogen-charging, both the tensile strength and elongation of the alloys decrease. The hydrogen embrittlement index, which is defined as $I_H = [(\delta_0 - \delta_H)/\delta_0] \times 100\%$ (δ_0 and δ_H — total elongation-to-failure of hydrogen-free and hydrogen-charged specimens, respectively), is I_H=25% for the HEA and I_H=17% for HEA-C. Therefore, carbon-alloying assists higher hydrogen-related increase of the yield strength and, at the same time, partially suppresses hydrogen-assisted loss of elongation-to-failure.

Fig. 3 shows the hydrogen desorption profiles obtained by the TDS of the HEA and HEA-C specimens. For both alloys, the TDS curve contains a single low-temperature peak with $T_{max} \approx 215 - 230$°C, which corresponds to diffusible hydrogen trapped in the crystal lattice and reversible hydrogen traps such as grain boundaries, vacancies, dislocations, etc. [9,16,18,19]. A comparison of the two TDS profiles testifies that the height of the peak for the HEA-C is twice lower than that for the interstitial-free alloy. This indicates that, in spite of a lower grain size and higher crystal lattice expansion, the content of the dissolved diffusible hydrogen in the HEA-C is much lower than that in HEA. This is consistent with the data obtained by the elemental analysis: 134 and 63 wppm of hydrogen were absorbed by HEA and HEA-C specimens, respectively. Notably, the height of TDS peak usually increases with decreasing grain size in conventional Fe-based alloys [20, 21] or unaffected by grain size in Cantor alloy [9]. Therefore, in carbon-free high-entropy alloys, the interstitial sites trap more hydrogen instead of grain boundaries [9]. This correlates with the results on the hydrogen-affected growth of the yield strength, i. e., hydrogen is largely dissolved in

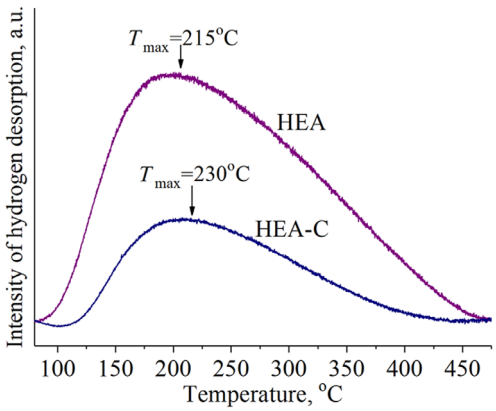

Fig. 3. (Color online) TDS spectra of hydrogen-charged HEA and HEA-C specimens.

the bulk of austenite grains (in interstitial sites). Hence, the presence of carbon in the solid solution reduces the hydrogen absorption capacity of the alloy rather than grain refinement. For conventional AISI 304 austenitic stainless steel, Dayal et al. [22] reported that increasing the carbon content from 0.045 to 0.085 wt.% reduces hydrogen diffusivity by a factor of 8. Hence, carbon-alloying of HEA causes a decrease in the hydrogen diffusivity in the alloy, reducing hydrogen accumulation during charging. But despite the lower concentration of hydrogen in the carbon-doped alloy, the $\Delta\sigma_{0.2}^{H}$ is greater compared to the interstitial-free Cantor alloy. This can be attributed to the nonuniform distribution of hydrogen atoms in the crystal lattice of HEA-C specimens. Since carbon atoms are prone to clustering and possess strong chemical affinity to chromium and manganese atoms, it causes a noticeable chemical microinhomogeneity in the solid-solution of the HEA-C alloy [23]. Due to this microinhomogeneity, hydrogen can be trapped in regions with a locally smaller lattice parameter (locally depleted by carbon, chromium and manganese). Therefore, at a lower hydrogen concentration in the solid-solution of HEA-C, hydrogen can cause higher lattice distortions compared to the homogeneous solid-solution of the Cantor alloy.

As shown in Fig. 4 a and d, the side surfaces of the fractured hydrogen-charged specimens undergo intensive cracking. Intergranular cracking dominates, but there is also a small fraction of transgranular cracks on the side surfaces of the HEA ana HEA-C specimens. It is interesting to note that the contribution of transgranular cracks is slightly reduced in the carbon-doped alloy in comparison with the interstitial-free one. In previous studies [10] we have reported that the number of hydrogen-assisted transgranular cracks significantly increases in nitrogen-alloyed HEA compared to nitrogen-free HEA. Such opposite effects of carbon and nitrogen on the cracking behavior in hydrogen-charged interstitial high-entropy alloys can be associated with their different influence on the stacking fault energy (SFE) and the dislocation arrangement of the alloys. Nitrogen contributes the formation of short-range order of atoms in solid-solution (promotes planar dislocation arrangement), while carbon leads to clustering with chromium and manganese atoms (assists wavy glide of the dislocations) [10, 23 – 25]. Similar to nitrogen, hydrogen has been reported to reduce the SFE and to enhance the planar dislocation arrangement in conventional Fe-based alloys [26, 27], which is usually associated with the

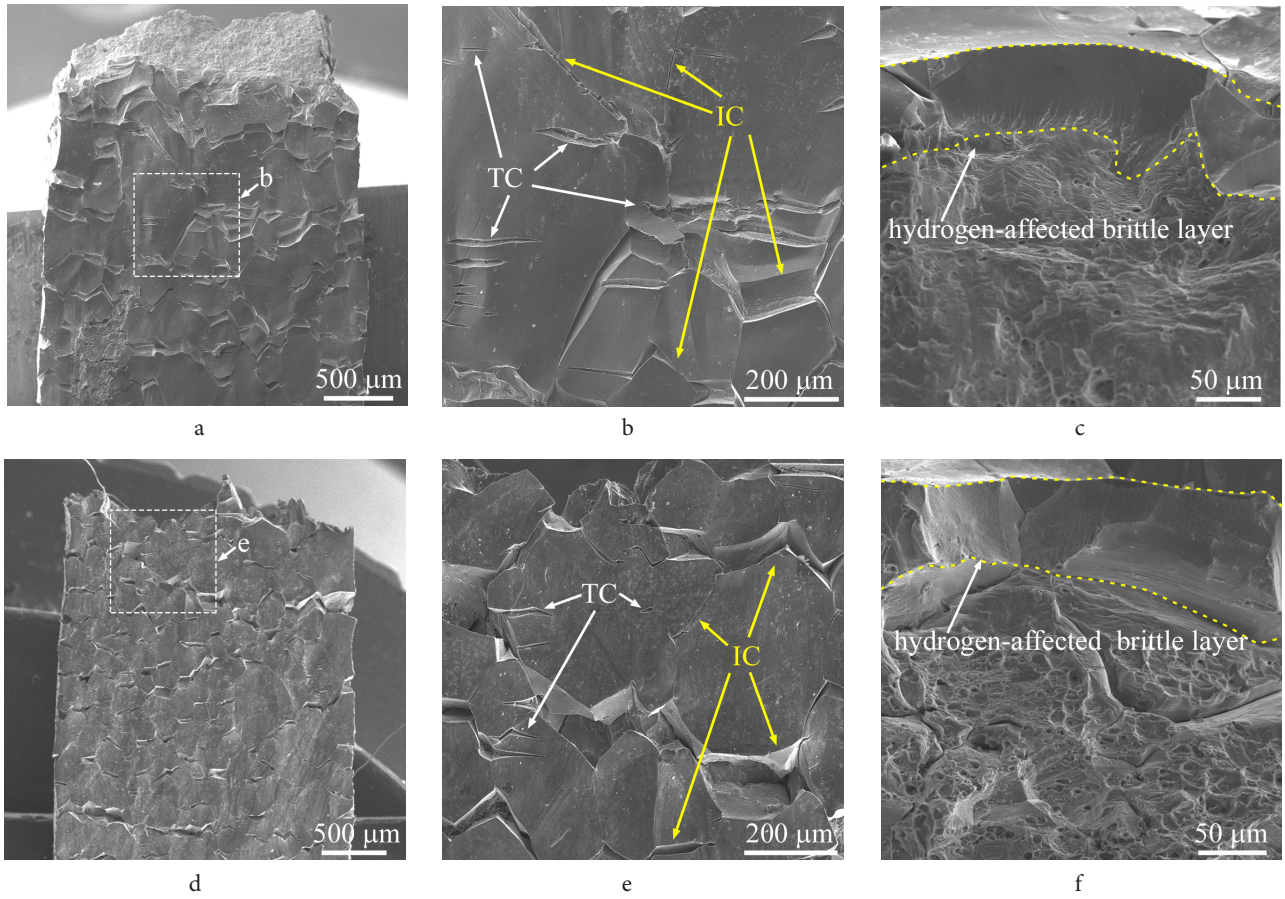

Fig. 4. SEM images of the side (a, b, d, e) and fracture (c, f) surfaces in hydrogen-charged HEA (a – c) and HEA-C (d – f) specimens after failure; TC — transgranular cracks, IC — intergranular cracks.

hydrogen enhanced localized plasticity (HELP) mechanism [28, 29]. The complementary effects of nitrogen-alloying and hydrogen-charging lead to the formation of quasi-cleavages and, consequently, transgranular cracks in austenitic grains. On the contrary, carbon-alloying increases the alloy's SFE [30, 31], thereby counteracting the effect of hydrogen and promoting a random distribution of dislocations (or wavy glide). Assuming the similar effects of carbon-alloying in multicomponent alloys and Fe-based alloys, this decreases the tendency to transgranular cracking in a hydrogen-charged HEA-C alloy.

On the fracture surface, a brittle hydrogen-assisted surface layer and a ductile central part (dimple fracture) are observed in specimens of both alloys (Fig. 4 c and f). The average thickness of the hydrogen-affected brittle layer is insufficiently lower in HEA-C ($W_H = 62 \pm 35$ μm) as compared to HEA ($W_H = 70 \pm 21$ μm). The brittle layers are inhomogeneous in depth, and their average thicknesses differ within the experimental error. However, this experimental fact does not characterize the depth of the hydrogen-saturated layer in the HEA and HEA-C specimens immediately after the charging since stress-induced diffusion of the hydrogen atoms and hydrogen transport by mobile dislocations occur during the following tensile deformation [10]. Therefore, further studies are needed to evaluate all contributions to the hydrogen-assisted layer thickness.

The fracture micromechanisms in the brittle layers are similar in both alloys, intergranular fracture dominates despite the predominant hydrogen trapping by the interstitial sites of the crystal lattice rather than grain boundaries during hydrogen-charging. Hydrogen-induced intergranular fracture of high-entropy alloys has been reported in a number of studies [8 – 10]. Grain-boundary cracking can be related to the accumulation of hydrogen near the grain boundaries during deformation due to the stress field and the hydrogen transport by dislocation to the boundaries. In turn, this reduces both the ability of neighboring grains to deform cooperatively and grain boundary cohesive energy [8].

To summarize, our experimental data show that carbon-alloying decreases the absorbed hydrogen content in HEA, and carbon-alloyed HEA is more resistant to hydrogen embrittlement compared to the HEA in tensile tests at room temperature. Indeed, the above mentioned experimental facts support the idea about the primary role of the structure of the solid-solution in hydrogen absorption, accumulation and embrittlement in the austenitic multicomponent systems. But this can be caused not only by the influence of carbon on the austenitic phase, but also by a decrease in the grain size. Some researchers have found that grain refinement contributes an increase in hydrogen embrittlement resistance [9, 21, 22]. The hydrogen-assisted crack growth resistance has been reported to be improved by grain refinement because of the reduction in stress concentration at grain boundaries in fine-grained specimens [9, 21]. Grain refinement could also favorably affect the hydrogen embrittlement of HEA-C specimens, which opens the perspective for further research.

4. Conclusions

The effect of carbon-alloying (1 at.%) on the hydrogen embrittlement susceptibility of a $Fe_{20}Mn_{20}Cr_{20}Ni_{20}Co_{20}$ (at.%) high-entropy Cantor alloy has been studied. The carbon-alloyed alloy has higher resistance to hydrogen embrittlement compared to the interstitial-free Cantor alloy. This is due to the smaller grain size in the HEA-C, as well as a decrease in the hydrogen absorption capacity of the alloy caused by carbon alloying. It has been experimentally established that the solid-solution strengthening of the carbon-doped alloy by hydrogen atoms is higher than that in the HEA specimens, despite the lower hydrogen content in the HEA-C specimens. Although the hydrogen-induced increase in the yield strength indicates significant hydrogen trapping in the crystal lattice, the failure mode of the surface hydrogen-affected layer is mainly intergranular in both alloys. This confirms that hydrogen is redistributed during deformation and accumulates near grain boundaries, which contributes to intergranular fracture due to the combined effect of the applied stress and the influence of hydrogen on dislocations (plasticity) and the grain boundary cohesive energy.

Acknowledgements. The research was supported by the Russian Science Foundation (project No. 20-19-00261). The studies were carried out using the equipment of the Nanotech Center for Collective Use (ISPMS SB RAS, Tomsk) and equipment of the Tomsk Regional Core Shared Research Facilities Centre of National Research Tomsk State University. The authors thank PhD (Physics and Mathematics) S. V. Astafurov, K. A. Reunova and A. S. Nifontov for their help in conducting experimental works and useful discussions.

References

1. P. Gong, J. Nutter, P.E.J. Rivera-Diaz-Del-Castillo, W.M. Rainforth. Sci. Adv. 6, 6152 (2020). Crossref
2. Y. Lu, H. Huang, X. Gao, C. Ren, J. Gao, H. Zhang, S. Zheng, Q. Jin, Y. Zhao, C. Lu. J. Mater. Sci. Technol. 35, 369 (2019). Crossref
3. Z. Wu, C.M. Parish, H. Bei. J. Alloys Compd. 647, 815 (2015). Crossref
4. F. Otto, A. Dloughy, Ch. Somsen, H. Bei, G. Eggeler, E.P. George. Acta. Mater. 61, 5743 (2013). Crossref
5. A. Gali, E.P. George. Intermetallics. 39, 74 (2013). Crossref
6. Y. Zhao, D.-H. Lee, M.-Y. Seok, J.-A. Lee, M.P. Phaniraj, J.-Y. Suh, H.-Y. Ha, J.-Y. Kim, U. Ramamurty, J.-i. Jang. Scr. Mater. 135, 54 (2017). Crossref
7. H. Luo, Z. Li, D. Raabe. Sci. Rep. 7, 9892 (2017). Crossref
8. K. Bertsch, K. Nygren, S. Wang, H. Bei, A. Nagao. Corros. Sci. 184, 109407 (2021). Crossref
9. M. Koyama, K. Ichii, K. Tsuzaki. Int. J. Hydrogen Energy. 44, 17163 (2019). Crossref
10. E. Astafurova, M. Panchenko, K. Reunova, A. Mikhno, V. Moskvina, E. Melnikov, S. Astafurov, H. Maier. Scripta Mater. 194, 113642 (2021). Crossref
11. J.Y. Ko, S.I. Hong. J. Alloys Compd. 743, 115 (2018). Crossref
12. E.V. Melnikov, S.V. Astafurov, K.A. Reunova, V.A. Moskvina, I.A. Tumbusova, M.Yu. Panchenko, E.G. Astafurova. Letters on Materials. 11 (4), 375 (2021). (in Russian) Crossref
13. E.G. Astafurova, E.V. Melnikov, K.A. Reunova. Phys. Mesomech. 24, 674 (2021). Crossref
14. H. Luo, Z. Li, W. Lu, D. Ponge, D. Raabe. Corros. Sci. 136, 403 (2018). Crossref
15. H. Luo, Z. Pan, X. Wang, H. Cheng, A.A. Nazarov, X. Li. Corros. Sci. 203, 110357 (2022). Crossref
16. Z. Fu, P. Wu, S. Zhu, K. Gan, D. Yan, Z. Li. Corros. Sci. 194, 109933 (2022). Crossref
17. E.G. Astafurova, E.V. Melnikov, S.V. Astafurov, K.A. Reunova, M.Yu. Panchenko, V.A. Moskvina, I. Tumbusova. Mater. Lett. 285, 129073 (2021). Crossref
18. R. Oriani. Acta Metall. 18, 147 (1970). Crossref
19. S. Frappart, A. Oudriss, X. Feaugas, J. Creus, J. Bouhattate. Scripta Mater. 65, 859 (2011). Crossref
20. Y. Bai, Y. Momotani, M.C. Chen, A. Shibata, N. Tsuji. Mater. Sci. Eng., A. 651, 935 (2016). Crossref
21. C. Park, N. Kang, S. Liu. Corros. Sci. 128, 33 (2017). Crossref
22. R.K. Dayal, H.J. Grabke. Mater. Technol. 71, 255 (2000). Crossref
23. V.G. Gavriljuk, A.L. Sozinov, A.G. Balanyuk, S.V. Grigoriev, O.A. Gubin, G.P. Kopitsa, V.V. Runov. Metal. Mater. Trans. A. 28 (11), 2195 (1997). Crossref
24. Y. Han, H. Li, H. Feng, K. Li, Y. Tian, Z. Jiang. J. Mater. Sci. Technol. 65, 210 (2021). Crossref
25. M. Klimova, D. Shaysultanov, A. Semenyuk, S. Zherebtsov, G. Salishchev, N. Stepanov. J. Alloys Compd. 849, 156633 (2020). Crossref
26. I.M. Robertson. Eng. Fract. Mech. 68, 671 (2001). Crossref
27. A.E. Pontini, J.D. Hermida. Scripta Mater. 37 (11), 1831 (1997). Crossref
28. M.L. Martin, J.A. Fenske, G.S. Liu, P. Sofronis, I.M. Robertson. Acta Mater. 59, 1601 (2011). Crossref
29. T. Neeraj, R. Srinivasan, J. Li. Acta Mater. 60, 5160 (2012). Crossref
30. Z. Li, C.C. Tasan, H. Springer, B. Gault, D. Raabe. Sci. Rep. 7, 40704 (2017). Crossref
31. R.E. Schramm, R.P. Reed. Metallurgical Transactions A. 6A, 1345 (1975). Crossref